Maximum Bound Principle and Energy-Stability-Preserving SPH Method for Solving the Allen-Cahn Equation

Huanzhu Yang, Rahmatjan Imin, Azhar Halik

Abstract—This paper presents a novel framework for constructing numerical schemes that preserve both the Maximum Bound Principle (MBP) and energy dissipation for the Allen-Cahn equation. We develop a class of Smoothed Particle Hydrodynamics (SPH) schemes for the Allen-Cahn equation, which are semi-implicit and conditionally stable. These schemes are rigorously analyzed for stability. The primary contributions of this work are twofold. First, in terms of methodological innovation, we pioneer the application of both standard and modified SPH methods to numerically solve the Allen-Cahn equation. Numerical experiments further verify the accuracy and robustness of the proposed methods. Second, we provide rigorous proofs that these schemes preserve the discrete MBP and maintain energy stability. Our framework extends existing theory for semi-linear parabolic equations and suggests directions for future research. This includes applying the method to broader classes of equations and developing unconditionally stable, higher-order accurate variants.

Index Terms—Allen-Cahn equation; SPH; Meshless particle method; Maximum Bound Principle; Energy dissipation law

I. INTRODUCTION

The Allen-Cahn (AC) equation, originally proposed by Allen and Cahn [1] to model phase separation in binary alloys, is a foundational phase-field equation with broad applications in materials science, image segmentation, and biomembrane modeling. Mathematically, it is a semi-linear parabolic partial differential equation (PDE) of the form:

$$\frac{\partial \mathbf{u}}{\partial t} = \varepsilon^2 \Delta \mathbf{u} - \mathbf{f}(\mathbf{u}) \tag{1}$$

where u(x,t) is the phase variable, ε controls interface thickness, and the nonlinear term f(u) derives from the

Manuscript received April 21, 2025; revised August 2, 2025.

This work was supported by National Natural Science Foundation of China, Grant No:12462028.

Huanzhu Yang is a postgraduate of the College of Mathematical and Systems Science, Xinjiang University, Urumqi 830017, China (e-mail: 596352335@qq.com).

Rahmatjan Imin is an associate professor of the College of Mathematical and Systems Science in Xinjiang University, Urumqi 830017, China (e-mail: rahmatjanim@xju.edu.cn).

Azhar Halik is an associate professor of the College of Mathematical and Systems Science, Xinjiang University, Urumqi 830017, China (corresponding author to provide phone:0991-8582482, e-mail: azhar@xju.edu.cn).

double-well potential $F(u) = \frac{1}{4}(1-u)^2$.

Key features of the AC equation include the following: (i)Strict energy dissipation: the total energy

$$E[\mathbf{u}] = \int_{\Omega} \left(\frac{\varepsilon^2}{2} |\nabla \mathbf{u}|^2 + F(\mathbf{u}) \right) dx$$
 (2)

decreases monotonically over time, i.e., $\frac{d E}{dt} \le 0$.

(ii)MBP: $u(x,t) \in [-1,1]$ if initialized within these bounds.

These properties impose strict requirements on numerical scheme design. In the numerical solution of the AC equation, the stability of its equilibrium points is of vital importance. According to relevant research [2], the equilibrium points should satisfy the energy dissipation and the MBP to ensure the long-term stability of the system and the rationality of the solutions.

The AC equation has undergone significant theoretical evolution-from foundational analysis (existence/uniqueness proofs via energy methods [3], stability of equilibria [4], and Γ -convergence to mean curvature flow [5]) to modern studies of sharp-interface limits, nonlocal variants, and multiphysics coupling (e.g., Navier-Stokes-Allen-Cahn [6] and Cahn-Hilliard-Allen-Cahn systems [7]). Its applications in image processing [8] and medicine [9] have expanded phase-field theory's interdisciplinary impact.

In numerical methods, spatial discretization critically affects accuracy and stability. Classical approaches like finite differences [10] and finite elements [11] achieve precision through structured grids but struggle with complex geometries. Recent advances include unconditionally stable high-order schemes [12] and AMR strategies [13] for interface resolution. While efficient, mesh-based methods face limitations with intricate domains and strong nonlinearities, motivating meshfree alternatives. Adam et al. demonstrated RBF methods for AC equations with complex boundaries [14], while deep learning frameworks like PINNs [15] extend applicability to high-dimensional nonlinear regimes. These approaches excel at handling evolving interfaces and complex geometries.

While meshfree approaches have gained traction in AC simulations, the SPH method remains largely unexplored, presenting both challenges and opportunities for methodology development.

This work introduces the first enhanced SPH method for

the AC equation discretization. By combining Taylor expansions with kernel moment properties, we develop derivative approximations eliminating traditional SPH's kernel differentiation requirement, yielding an efficient linear discrete model. Theoretical analysis proves the scheme preserves both MBP and energy dissipation with reasonable time-steps. Numerical experiments confirm robustness for complex geometries and long-term simulations, establishing a new meshfree phase-field modeling framework.

II. SPATIAL APPROXIMATION

A. Conventional SPH Methodology

The conventional SPH technique employs two principal computational phases for function approximation [16]:

(i)Kernel Approximation: The field quantity u(x) is approximated by the convolution integral:

$$\langle \mathbf{u}(x) \rangle = \int_{\Omega} \mathbf{u}(x') \mathbf{W}(x - x', h) dx'$$
 (3)

where W(x-x',h) denotes the smoothing kernel with compact support, the parameter h controls the kernel's smoothing length, while Ω defines its support region where $W(x-x',h) \neq 0$. When W(x-x',h) is sufficiently smooth (e.g., C^{∞}), the generalized derivative estimate becomes:

$$\left\langle \frac{\partial^{k} \mathbf{u}(x)}{\partial x^{k}} \right\rangle = \frac{1}{h^{d}} \int_{\Omega} \mathbf{u}(x') \frac{\partial^{k} \mathbf{W}(x-x',h)}{\partial x^{k}} dx' \tag{4}$$

(ii)Particle Approximation: The integral is approximated by particle discretization:

$$\langle \mathbf{u}(x) \rangle = \sum_{j=1}^{m_j} \frac{m_j}{\rho_j} \mathbf{u}(x_j) \mathbf{W}(x - x', h)$$
 (5)

where j indexes neighboring particles within Ω . The particle approximation for the gradient is constructed as:

$$\left\langle \frac{\partial^{k} \mathbf{u}(x)}{\partial x^{k}} \right\rangle = \sum_{j} \frac{m_{j}}{\rho_{j}} \mathbf{u}(x_{j}) \frac{\partial^{k} \mathbf{W}(x - x_{j}, h)}{\partial x^{k}}$$
(6)

The accuracy of this approximation depends on the kernel function, particle density, and smoothing length.

B. KDF-SPH Methodology

Building upon the conventional SPH framework, we now present the Kernel Derivative-Free SPH (KDF-SPH) approach that circumvents kernel differentiation. This methodology combines Taylor expansion with statistical moment properties of kernel functions to directly construct derivative approximations, thereby eliminating the need for traditional kernel function differentiation [17].

The expansion of u(x') about reference point x yields:

$$\mathbf{u}(x') = \mathbf{u}(x) + (x - x') \cdot \nabla \mathbf{u}(x)$$
$$+ \frac{1}{2} (x - x')^{\mathsf{T}} \cdot \Delta \mathbf{u}(x) \cdot (x - x') + \cdots$$
(7)

Kernel moments $M_n^{k_1 \cdots k_n} \in L^1(\Omega)$ are introduced, defined as:

$$M_n^{k_1 \cdots k_n} = \frac{1}{h^d} \int_{\Omega} \left(\frac{x_{k_1} - x_{k_1}'}{h} \right) \cdots \left(\frac{x_{k_n} - x_{k_n}'}{h} \right) W\left(\frac{x - x'}{h} \right) dx' (8)$$

These moments depend solely on the shape of kernel function W(x-x',h) and are independent of the smoothing length h.

The Taylor expansion is multiplied by $\frac{x-x'}{h}W(x-x',h)$ and integrated over the kernel support domain, yielding:

$$\left\langle \frac{x_k - x_k'}{h} \mathbf{u}(x) \right\rangle = M_1^k \mathbf{u}(x) + h M_2^{\alpha k} \frac{\partial \mathbf{u}(x)}{\partial x_\alpha} + o(h^2) \quad (9)$$

For symmetric kernels (where $M_1^k = 0$), the first derivative is derived as:

$$\frac{\partial \mathbf{u}(x)}{\partial x_{\alpha}} = \frac{1}{h M_{2}^{\alpha k}} \left\langle \frac{x_{k} - x_{k}'}{h} \mathbf{u}(x) \right\rangle + o(h^{2})$$
 (10)

The continuous form is discretized into a matrix operation $\mathbf{U} = \mathbf{A}\mathbf{X} + o(h^2)$, where \mathbf{A} is KDF-SPH discretization matrix constructed from particle positions and kernel values, that is,

$$\mathbf{U} = \left(\frac{\partial \mathbf{u}(x_{1})}{\partial x}, \dots, \frac{\partial \mathbf{u}(x_{n})}{\partial x}\right)^{\mathrm{T}}, \quad \mathbf{X} = \left(\mathbf{u}(x_{1}), \dots, \mathbf{u}(x_{n})\right)^{\mathrm{T}}$$

$$\mathbf{A} = \frac{1}{hM_{2}} \begin{pmatrix} \frac{m_{1}}{\rho_{1}} \frac{x_{1} - x_{1}}{h} \mathbf{W}_{11} & \dots & \frac{m_{n}}{\rho_{n}} \frac{x_{n} - x_{1}}{h} \mathbf{W}_{1n} \\ \vdots & \ddots & \vdots \\ \frac{m_{1}}{\rho_{1}} \frac{x_{1} - x_{n}}{h} \mathbf{W}_{n1} & \dots & \frac{m_{n}}{\rho_{n}} \frac{x_{n} - x_{n}}{h} \mathbf{W}_{nn} \end{pmatrix}$$

$$(11)$$

Higher-order terms are incorporated by multiplying the Taylor expansion by $\left(\frac{x-x'}{h}\right)^2$ W (x-x',h) and integrating:

$$\left\langle \left(\frac{x_k - x_k'}{h} \right)^2 \mathbf{u}(x) \right\rangle = M_2^{kk} \mathbf{u}(x) + \frac{h^2}{2} M_4^{\alpha \alpha kk} \frac{\partial^2 \mathbf{u}(x)}{\partial x_\alpha^2} + o(h^2)$$

$$(12)$$

Simplifying with $M_4^{\alpha\beta kl} = 0, \alpha \neq \beta$, the second-order derivative becomes:

$$\frac{\partial^{2} \mathbf{u}(x)}{\partial x_{a}^{2}} = \frac{1}{h^{2} M_{4}^{\alpha \alpha k k}} \left\langle \left(\frac{x_{k} - x_{k}'}{h}\right)^{2} \mathbf{u}(x) - M_{2}^{k k} \mathbf{u}(x) \right\rangle + o(h^{2})$$

$$(13)$$

Similar to first derivatives, this is discretized into matrix form, avoiding explicit computation of kernel derivatives.

For multi-dimensional problems, directional moments (e.g., M_2^{xx}, M_2^{yy}) are combined to construct gradient or Laplacian operators, and mixed moments (e.g., M_4^{xxyy}) are

used to handle cross-derivatives like $\frac{\partial^2 \mathbf{u}(x, y, t)}{\partial x \partial y}$.

III. THEORETICAL ANALYSIS

To simplify the notation, we define the standard Sobolev space with homogeneous Dirichlet conditions, their norms and inner products using the symbols $H^k\left(\Omega\right)$, $\left\|\cdot\right\|_k$ and $\left(\cdot,\cdot\right)$ respectively. To be specific, $\left\|\cdot\right\|_2$ and $\left(\cdot,\cdot\right)$ are used to represent the norm and inner product of $L_2\left(\Omega\right)$, and $\left\|\cdot\right\|_\infty$ for the norm of $L_\infty\left(\Omega\right)$. The domain is the set of uniformly spaced particles in square $\begin{bmatrix}0,1\end{bmatrix}^2$ or cubic $\begin{bmatrix}0,1\end{bmatrix}^3$, but the analysis can extend to domains with different shapes. We regard X as the solution space spanned by the particle-based function u_k , where $X \cong R^N$ and $\partial X \cong R^2$.

A. The semi-discrete maximum bound principle

Following Du et al.'s abstract framework for the AC equation's MBP [18], proper spatial discretization of such semi-linear parabolic equations yields the following ODE system:

$$\frac{d\mathbf{u}}{dt} = L\mathbf{u} + N[\mathbf{u}] \tag{14}$$

where $L\mathbf{u}$, $N\mathbf{u}$ represents the linear and non-linear components, respectively. Building upon this framework, we initially restrict the KDF-SPH-based numerical solution of the AC equation to the spatial discretization framework for proof simplification.

The KDF-SPH approximation of the Laplace operator (13) generates the sparse matrix \mathbf{K}_2 with entries:

$$\mathbf{K}_{2} = \begin{bmatrix} \frac{m_{1}}{\rho_{1}} \left(\frac{x_{1} - x_{1}}{h}\right)^{2} W_{11} - \sum_{j=1}^{N} \frac{m_{j}}{\rho_{j}} \left(\frac{x_{j} - x_{1}}{h}\right)^{2} W_{1j} & \dots & \frac{m_{N}}{\rho_{N}} \left(\frac{x_{1} - x_{N}}{h}\right)^{2} W_{1N} \\ \frac{\sum_{j=1}^{N} \frac{m_{j}}{\rho_{j}} \left(\frac{x_{j} - x_{1}}{h^{2}}\right)^{4} W_{1j} & \dots & \frac{\sum_{j=1}^{N} \frac{m_{j}}{\rho_{j}} \left(\frac{x_{j} - x_{1}}{h^{2}}\right)^{4} W_{1j} \\ \vdots & \ddots & \vdots \\ \frac{m_{1}}{\rho_{1}} \left(\frac{x_{1} - x_{N}}{h}\right)^{2} W_{N1} & \dots & \frac{m_{N}}{\rho_{N}} \left(\frac{x_{N} - x_{N}}{h}\right)^{2} W_{NN} - \sum_{j=1}^{N} \frac{m_{j}}{\rho_{j}} \left(\frac{x_{j} - x_{N}}{h}\right)^{2} W_{Nj} \\ \frac{\sum_{j=1}^{N} \frac{m_{j}}{\rho_{j}} \left(\frac{x_{j} - x_{N}}{h^{2}}\right)^{4} W_{Nj} & \dots & \frac{\sum_{j=1}^{N} \frac{m_{j}}{\rho_{j}} \left(\frac{x_{j} - x_{N}}{h}\right)^{2} W_{Nj} \end{bmatrix}$$

and the elements are expressed as k_{ii} , $1 \le i, j \le N$.

The kernel function W_{ij} adopts the cubic B-spline kernel function:

$$W(x-x',h) = \frac{\alpha_d}{h^d} \begin{cases} \frac{2}{3} - s^2 + \frac{1}{2}s^3 & 0 \le s < 1\\ \frac{1}{6}(2-s)^3 & 1 \le s < 2\\ 0 & s \ge 2 \end{cases}$$
 (16)

where $q = \frac{r}{h}$, r = |x - x'| is the is the distance between points x and x'; h is the smoothing length.

The cubic B-spline kernel function possesses three key characteristics: non-negativity, symmetry, and compact support. That is,

$$W_{ij} \ge 0; W_{ij} = W_{ji}$$
 (17)

Due to the uniform particle distribution, each particle i has at least one neighboring particle j satisfying $W_{ij}>0$ with $x_i\neq x_j$, meaning there exist no isolated points in Ω . Therefore, \mathbf{K}_2 is weakly diagonally dominant:

$$|k_{ii}| = \sum |k_{ij}|; k_{ii} < 0, k_{ij} \ge 0$$
 (18)

The discrete matrix \mathbf{K}_2 can be extended to two and three dimensions through the Kronecker tensor product formulation.

By discretizing the AC equation (1) using KDF-SPH, we obtain an ODE system similar to (14):

$$\frac{d\mathbf{u}}{dt} = \mathbf{A}\mathbf{u} + \mathbf{f}_h(\mathbf{u}), \forall t > 0$$
 (19)

where $\mathbf{A} = \varepsilon^2 \mathbf{K}_2$,and the elements are expressed as a_{ij} , $1 \le i, j \le N$.

In order to establish the MBP for this equation, we propose the following assumption.

Assumption: The non-linear operator discretization f_h acts as a composite function induced by a given one-variable continuously differentiable function $f: R \mapsto R$, that is,

$$f_h[u](x) = f_0(u(x)), \forall u \in X$$
 (20)

There exists a constant $\gamma \ge 0$ such that

$$f_0(\gamma) \le 0 \le f_0(-\gamma)$$
 (21)

The key to the assumption is that the nonlinear operator f has opposite signs on the left and right sides of 0.

Lemma 1: Under Assumption 1, the discrete linear operator **A** generates a contraction semigroup $\{e^{t\mathbf{A}}\}_{t>0}$.

Proof:

(i)Consider any $u \in X$ and let x_k be the point where |u(x)| achieves its supremum, which implies $||u_k||_{\infty} = |u(x_k)|$. The non-negative case $u_k \ge 0$ suffices for our analysis by definition:

$$\mathbf{A} \mathbf{u}_{k} = a_{kk} \mathbf{u}_{k} + \sum_{\substack{j=1\\j \neq k}}^{N} a_{kj} \mathbf{u}_{j}$$
 (22)

Since $u_j \le u_k (k \ne j)$ and condition (18), we have

$$\sum_{\substack{j=1\\j\neq k}}^{N} a_{kj} \mathbf{u}_{j} \le \left(\sum_{\substack{j=1\\j\neq k}}^{N} a_{kj}\right) \mathbf{u}_{k} = -a_{kk} \mathbf{u}_{k}$$
 (23)

Therefore, we obtain:

$$\mathbf{A} \mathbf{u}_{k} = a_{kk} \mathbf{u}_{k} + \sum_{\substack{j=1\\j \neq k}}^{N} a_{kj} \mathbf{u}_{j} \le a_{kk} \mathbf{u}_{k} - a_{kk} \mathbf{u}_{k} = 0$$
 (24)

Condition (24) implies that matrix **A** is dissipative.

(ii) From the Lumer-Phillips Theorem and condition (18), it follows that: for any constant $\alpha > \max_k \alpha_{kk}$, then it holds:

$$\alpha - a_{kk} \ge \alpha - |a_{kk}| = \alpha - \sum_{\substack{j=1\\j \ne k}}^{N} |a_{kj}| = -\sum_{\substack{j=1\\j \ne k}}^{N} |a_{kj}|$$
 (25)

This shows that matrix $\alpha \mathbf{I} - \mathbf{A}$ is strictly diagonally dominant and hence invertible, where \mathbf{I} is the N × N identity matrix.

(iii)Under condition (18),as matrix A has non-negative off-diagonal terms, the resulting $e^{t\mathbf{A}} = \sum_{n=0}^{\infty} \frac{(t\mathbf{A})^n}{n!}$ inherits this non-negative off-diagonal characteristic; as the row sums of matrix A vanish, we have $\mathbf{A} \cdot \mathbf{1} = \mathbf{0}$ and $e^{t\mathbf{A}} = \mathbf{1}$. That is,

$$(e^{t\mathbf{A}} \mathbf{u})_{i} = \sum_{j=1}^{N} (e^{t\mathbf{A}})_{ij} \mathbf{u}_{j} \le \sum_{j=1}^{N} (e^{t\mathbf{A}})_{ij} \mathbf{u}_{k} = \mathbf{u}_{k} (e^{t\mathbf{A}} \mathbf{1})_{i} = \mathbf{u}_{k}$$
 (26)

i.e., $\|e^{t\mathbf{A}}\|_{\infty} \le \|\mathbf{u}_k\| = \|\mathbf{u}\|_{\infty}$ completing the proof.

Lemma 2: Under Assumption, we have:

$$\frac{d}{dt} \left[\max_{i} u_{i}(t) \right] \leq f \left[\max_{i} u_{i}(t) \right] \\
\frac{d}{dt} \left[\min_{i} u_{i}(t) \right] \geq f \left[\min_{i} u_{i}(t) \right]$$
, $\forall t > 0$ (27)

Proof:

Let $u_{max}(t) = \max_{1 \le i \le N} u_i(t)$, we suppose that u(x,t) reaches its maximum at (x_k, t^*) , i.e.,

$$\mathbf{u}_{k}\left(t^{*}\right) = \mathbf{u}_{\max}\left(t^{*}\right); \mathbf{u}_{i}\left(t^{*}\right) \le \mathbf{u}_{k}\left(t^{*}\right). \forall i \ne k$$
 (28)

Inserting this into the semi-discrete system (19):

$$\frac{d}{dt}\mathbf{u}_{k}\left(t^{*}\right) = \left(\mathbf{A}\,\mathbf{u}\left(t^{*}\right)\right)_{k} + \mathbf{f}\left(\mathbf{u}_{k}\left(t^{*}\right)\right) \tag{29}$$

Expanding the matrix-vector product yields:

$$\left(\mathbf{A}\mathbf{u}\left(t^{*}\right)\right)_{k} = \sum_{j=1}^{N} \mathbf{A}_{kj} \mathbf{u}_{j}\left(t^{*}\right)$$

$$= \mathbf{A}_{kk} \mathbf{u}_{k}\left(t^{*}\right) + \sum_{\substack{j=1\\j\neq k}}^{N} \mathbf{A}_{kj} \mathbf{u}_{j}\left(t^{*}\right)$$
(30)

Combine condition (18) and (28), we obtain:

$$\left(\mathbf{A}\,\mathbf{u}\left(t^{\,*}\right)\right)_{\iota} \le 0\tag{31}$$

Consequently, (29) reduces to $\frac{d}{dt}\mathbf{u}_{k}\left(t^{*}\right) \leq \mathbf{f}\left(\mathbf{u}_{k}\left(t^{*}\right)\right)$, which gives

$$\frac{d}{dt} \left[\max_{i} \mathbf{u}_{i}(t) \right] \le f \left[\max_{i} \mathbf{u}_{i}(t) \right], \quad \forall t > 0$$
 (32)

On the other hand, let $\mathbf{u}_{\min}(t) = \min_{1 \le i \le N} \mathbf{u}_i(t)$, we suppose that $\mathbf{u}(x,t)$ reaches its minimum at (x_m,t^{**}) , a similar analysis yields to obtain $(\mathbf{A}\mathbf{u}(t^{**}))_m \ge 0$ and

$$\frac{d}{dt} \left[\min_{i} \mathbf{u}_{i}(t) \right] \ge f \left[\min_{i} \mathbf{u}_{i}(t) \right], \quad \forall t > 0$$
 (33)

Hence, the proof is complete.

We have now established the existence and uniqueness of solutions to the model problem (1) that maintain the MBP property. The following theorem summarizes our main result:

Theorem 1: Consider the semi-discrete AC system (19) under Dirichlet boundary conditions. For arbitrary T > 0, when **A** complies with Condition (18) and Lemma 1, while f(u) satisfies Assumption and Lemma 2, if both the initial is bounded by 1, i.e., $\|u_0(x)\|_{\infty} \le 1$, then the solution to the discrete scheme exists, is unique, and satisfies

$$\|\mathbf{u}_h(x,t)\|_{\infty} \le 1, \quad \forall t \in (0,T]$$

Proof:

Using Condition(19) and Lemma 1, As \mathbf{A} is the generator of a contraction semigroup, the Banach fixed-point theorem yields local existence and uniqueness of solutions to the semi-discrete AC system on $[0,t_1]$. Global existence up to arbitrary T>0 follows from standard continuation arguments.

Let $\mathbf{u}_{\max}\left(t\right) = \max_{1 \le i \le N} \mathbf{u}_{i}\left(t\right)$, we suppose there exist some time t^* makes $\mathbf{u}_{\max}\left(t^*\right) \ge \gamma$. The continuity argument guarantees the existence of a first hitting time t_0 at which

$$\mathbf{u}_{\max}\left(t_{0}\right) = \gamma, \frac{d}{dt}\mathbf{u}_{\max}\left(t_{0}\right) \ge 0 \tag{35}$$

Combining the above conclusion with the Assumption and Lemma 2, we obtain that

$$\frac{d}{dt}\mathbf{u}_{\max}\left(t_{0}\right) \le \mathbf{f}\left(\mathbf{u}_{\max}\left(t_{0}\right)\right) = \mathbf{f}\left(\gamma\right) \le 0 \tag{36}$$

which contradicts $\frac{d}{dt}\mathbf{u}_{\max}\left(t_{0}\right)\geq0$ unless $\frac{d}{dt}\mathbf{u}_{\max}\left(t_{0}\right)=0$ holds. In this case, $\mathbf{u}_{\max}\left(t\right)$ reaches its critical value γ at t_{0} and cannot grow further. Similarly,

$$\frac{d}{dt}\mathbf{u}_{\min}(t) \ge f\left(\mathbf{u}_{\min}(t)\right) = f\left(-\gamma\right) \ge 0 \tag{37}$$

 $\mathbf{u}_{\min}(t)$ reaches its critical value $-\gamma$.

From [18], $\gamma = 1$, which means $-1 \le u_h(x,t) \le 1$. The theorem is proved.

B. The fully discrete maximum bound principle

To achieve better numerical results while avoiding overly complex computational procedures, we adopt the Crank-Nicolson (CN) scheme for the linear term and an explicit scheme for the nonlinear term. Therefore, the fully discrete scheme for the equation (1) is written as:

$$\frac{\mathbf{u}^{n+1} - \mathbf{u}^n}{dt} = \frac{\mathbf{A}}{2} \cdot \left(\mathbf{u}^{n+1} + \mathbf{u}^n \right) + \mathbf{f} \left(\mathbf{u}^n \right)$$
 (38)

where $f(u) = u^3 - u$, the derivative of the double-well potential $F(u) = \frac{1}{4}(u^2 - 1)^2$. After reformatting, (38) can be rewritten as

$$\left(\mathbf{I} - dt \cdot \frac{\mathbf{A}}{2}\right) \mathbf{u}^{n+1} = \left(\mathbf{I} + dt \cdot \frac{\mathbf{A}}{2}\right) \mathbf{u}^{n} + dt \cdot f\left(\mathbf{u}^{n}\right)$$
(39)

Clearly, (39) is equivalent to (38). We now present the fully discrete MBP:

Theorem 2: Let T>0 be arbitrary. Under the requirements that **A** complies with condition (18) and Lemma 1, while f(u) satisfies Assumption and Lemma 2, the fully discrete scheme (38) preserves the MBP provided the time-step satisfies $dt \le \frac{1}{2}$. That is, if $\|u^0\|_{\infty} \le 1$ holds, then $\|u^{n+1}\|_{\infty} \le 1$ follows for any $n \ge 0$.

Proof:

Theorem 2 establishes the stability of the spatially discrete system. Through proper time-step selection, this stability property extends to the fully discrete scheme (39), guaranteeing the preservation of the discrete MBP.

Let $\mathbf{B} = \mathbf{I} - dt \cdot \frac{\mathbf{A}}{2}$. The elements of matrix \mathbf{B} are defined

$$b_{ij} = \begin{cases} 1 + \frac{dt \cdot \varepsilon^{2}}{2} k_{ij} = 1 + \frac{dt \cdot \varepsilon^{2}}{2} \frac{1}{\sum_{j=1}^{N} (x_{j} - x_{i})^{2}}, & i = j \\ -\frac{dt \cdot \varepsilon^{2}}{2} k_{ij} = -\frac{dt \cdot \varepsilon^{2}}{2} \frac{\frac{m_{j}}{\rho_{j}} \left(\frac{x_{j} - x_{i}}{h}\right)^{2} W_{ij}}{\sum_{j=1}^{N} \frac{m_{j}}{\rho_{j}} \left(x_{j} - x_{i}\right)^{4}} W_{ij}, & i \neq j \end{cases}$$

$$(40)$$

Clearly, it satisfies:

$$b_{ii} \ge 1 > 0, b_{ii} \le 0 \tag{41}$$

$$|b_{ii}| - \sum_{j=1}^{N} |b_{ij}| = 1 + \frac{dt \cdot \varepsilon^{2}}{2} |k_{ii}| - \sum_{\substack{j=1 \ j \neq i}}^{N} \frac{dt \cdot \varepsilon^{2}}{2} |k_{ij}|$$

$$= 1 + \frac{dt \cdot \varepsilon^{2}}{2} \sum_{i=1}^{N} |k_{ij}| = 1 > 0$$
(42)

Conditions (41)-(42) show that matrix **B** possesses the M-matrix property and is therefore invertible. Consequently, the numerical scheme (39) possesses a unique solution.

Assuming
$$\|\mathbf{u}^n\|_{\infty} \le 1$$
 holds. Let $\psi = \left(\mathbf{I} + \frac{dt}{2}\mathbf{A}\right)\mathbf{u}^n$. It's evident that the off-diagonal elements of matrix $\mathbf{I} + \frac{dt}{2}\mathbf{A}$ are non-negative and its row sums equal 1. Thus, $|\mathbf{u}_i^n| \le 1$ implies

Let $\omega = \psi + dt \cdot f(u^n)$, then we have $|\omega_i| \le 1 + dt \cdot |f(u_i^n)|$. Combining the assumptions, $\omega_i \le 1$ holds when $u_i^n = 1$; $\omega_i \ge -1$ holds when $u_i^n = -1$. To ensure $|\omega| \le 1$ holds for all $||u||_{\infty} \le 1$, we have to ensure all the extremum points lie within the interval [-1,1]. Through analysis, the condition is satisfied if $dt \le \frac{1}{\max_{|u| \le 1} |f'(u)|}$. From

[19, Example 2.1]
$$L = 2$$
, we know that $\max_{|\mathbf{u}| \le 1} |\mathbf{f}'(\mathbf{u})| = 2$.

In summary, when $dt \le \frac{1}{2}$, for any ω satisfies $|\omega_i| \le 1$, we have $\mathbf{u}^{n+1} = \mathbf{B}^{-1}\omega$, that makes $|\mathbf{u}_i^{n+1}| \le 1$ which means $\|\mathbf{u}^{n+1}\|_{\infty} \le 1$ holds.

The Theorem is proved.

 $|\psi_i| \leq 1$.

C. Energy Stability

The AC equation constitutes the L^2 -gradient flow for the energy functional (2), and it obeys the following energy dissipation property. The discrete formulation of the energy functional (2) is given by [20]:

$$E_h(u) = \frac{\varepsilon^2}{2} (\nabla_h u, \nabla_h u)_h + (F(u), 1)_h$$
 (43)

Preservation of energy dissipation by the discretization (38) requires rigorous verification. To this end, we derive the weak form of the KDF-SPH discretization.

First, let us provide a detailed exposition of the discretization methodology for scheme (38):

$$\frac{\mathbf{u}_{i}^{n+1} - \mathbf{u}_{i}^{n}}{dt} = \varepsilon^{2} \sum_{i} \frac{m_{j}}{\rho_{i}} \left(\mathbf{u}_{j}^{n+\frac{1}{2}} - \mathbf{u}_{i}^{n+\frac{1}{2}} \right) \mathbf{W}_{ij} + \mathbf{f} \left(\mathbf{u}_{i}^{n} \right)$$
(44)

where $\mathbf{u}^{\frac{1}{2}} = \frac{\mathbf{u}^{n+1} - \mathbf{u}^n}{2}$, $\mathbf{W}_{ij} = \mathbf{W}(\|\mathbf{x}_i - \mathbf{x}_j\|, h)$ represents the cubic B-spline kernel function. We now define the following discrete inner products:

$$\left(\mathbf{u},\mathbf{v}\right)_{h} = \sum_{i} m_{i} \,\mathbf{u}_{i} \,\mathbf{v}_{i} \tag{45}$$

And the gradient-based product:

$$(\nabla \mathbf{u}, \nabla \mathbf{v})_h = \sum_{i,j} \frac{m_i m_j}{\rho_i \rho_j} (\mathbf{u}_j - \mathbf{u}_i) (\mathbf{v}_j - \mathbf{v}_i) \mathbf{W}_{ij}$$
 (46)

The properties of W_{ij} directly imply that the discrete gradient product satisfies:

(i) Symmetry:

$$(\nabla \mathbf{u}, \nabla \mathbf{v})_{\iota} = (\nabla \mathbf{v}, \nabla \mathbf{u})_{\iota}$$

(ii) Non-negativity:

$$\left(\nabla \mathbf{u}, \nabla \mathbf{u}\right)_{h} = \sum_{i,j} \frac{m_{i} m_{j}}{\rho_{i} \rho_{j}} \left(\mathbf{u}_{j} - \mathbf{u}_{i}\right)^{2} \mathbf{W}_{ij} \geq 0$$

The KDF-SPH method admits a weak formulation due to (i) and(ii), which allows the energy stability to be proven analogously. This yields the weak formulation of the discretized AC equation:

$$\frac{1}{dt} \left(\mathbf{u}^{n+1} - \mathbf{u}^{n}, \mathbf{v} \right) + \varepsilon^{2} \left(\nabla \mathbf{u}^{n+\frac{1}{2}}, \nabla \mathbf{v} \right) + \left(\mathbf{f} \left(\mathbf{u}^{n} \right), \mathbf{v} \right) = 0,$$

$$\forall \mathbf{v} \in H_{1} \left(\Omega \right)$$

Theorem 3: Let T > 0 be arbitrary. For $dt \le 1$, the solution of (47) satisfies:

$$E_h(u^{n+1}) \le E_h(u^n), \forall n \ge 0$$

Proof.

Taking $\mathbf{v} = \mathbf{u}^{n+1} - \mathbf{u}^n$ where $\left| \mathbf{u}_i^{n+1} \right| \le 1$ and use the identity $(a,b) = \left| a \right|^2 - \left| b \right|^2$. The second term on the left-hand side of equation (47) is:

$$\varepsilon^{2} \left(\nabla \mathbf{u}^{n+\frac{1}{2}}, \nabla \mathbf{v} \right) = \frac{\varepsilon^{2}}{2} \left(\nabla \left(\mathbf{u}^{n+1} + \mathbf{u}^{n} \right), \nabla \left(\mathbf{u}^{n+1} - \mathbf{u}^{n-1} \right) \right)$$

$$= \frac{\varepsilon^{2}}{2} \left(\left\| \nabla \mathbf{u}^{n+1} \right\|_{2}^{2} - \left\| \nabla \mathbf{u}^{n} \right\|_{2}^{2} \right)$$

$$(48)$$

For the third term on the left hand of (47), we use the Taylor expansion

$$F\left(\mathbf{u}^{n+1}\right) - F\left(\mathbf{u}^{n}\right) \approx f\left(\mathbf{u}^{n}\right) \cdot \left(\mathbf{u}^{n+1} - \mathbf{u}^{n}\right) + \frac{f'\left(\varsigma^{n}\right)}{2} \cdot \left(\mathbf{u}^{n+1} - \mathbf{u}^{n}\right)^{2}, \varsigma^{n} \in \left(\mathbf{u}^{n}, \mathbf{u}^{n+1}\right)$$

$$(49)$$

and the condition that the derivative of the double-well potential satisfies $\max_{|\mathbf{u}|\leq 1} |\mathbf{f}'(\mathbf{u})| \leq L$ with Lipschitz constant $L\geq 2$. Based on the above derivation, we set the Lipschitz constant L=2.

Thus, we obtain:

$$(f(u^n), v) = (f(u^n), u^{n+1} - u^n)$$

$$= (F(u^{n+1} - u^n), 1) - \frac{1}{2} (f'(\varsigma^n)(u^{n+1} - u^n), u^{n+1} - u^n)$$
(50)

In summary, we may write (44) in the form:

$$\frac{1}{dt} \left\| \mathbf{u}^{n+1} - \mathbf{u}^{n} \right\|_{2}^{2} + \frac{\varepsilon^{2}}{2} \left(\left\| \nabla \mathbf{u}^{n+1} \right\|_{2}^{2} - \left\| \nabla \mathbf{u}^{n} \right\|_{2}^{2} \right) + \left(F\left(\mathbf{u}^{n+1}\right) - F\left(\mathbf{u}^{n}\right), 1 \right) \\
= \frac{1}{2} \left(f'\left(\varsigma^{n}\right) \left(\mathbf{u}^{n+1} - \mathbf{u}^{n}\right), \mathbf{u}^{n+1} - \mathbf{u}^{n} \right) \le \left\| \mathbf{u}^{n+1} - \mathbf{u}^{n} \right\|_{2}^{2} \tag{51}$$

Combining (48) with (51):

$$\frac{1}{dt} \left\| \mathbf{u}^{n+1} - \mathbf{u}^{n} \right\|_{2}^{2} + \mathbf{E}_{h} \left(\mathbf{u}^{n+1} \right) - \mathbf{E}_{h} \left(\mathbf{u}^{n} \right) \le \left\| \mathbf{u}^{n+1} - \mathbf{u}^{n} \right\|_{2}^{2}$$
 (52)

when $dt \le 1$.

This completes the proof.

D. Remark on Convergence Order

Having established the energy dissipation property, we now address the convergence order of the proposed scheme. The spatial discretization of the Laplacian operator via KDF-SPH (Eq. 13) preserves the second-order accuracy $\left(O\left(h^2\right)\right)$ demonstrated in [16] for general derivative approximations, as rigorously proven in [16, Theorems 1–2]. When coupled with the second-order Crank-Nicolson temporal discretization $\left(O\left(dt^2\right)\right)$, the full scheme achieves

an overall convergence rate of $(O(h^2 + dt^2))$, provided the time-step satisfies $dt \le 0.5$ (Theorem 2). This theoretical order is numerically validated in Section IV (Example 2), where error reduction under spatial refinement aligns with the expected rate. The Lipschitz continuity of f(u) with L=2 ensures the nonlinear term does not degrade this convergence behavior, as guaranteed by the energy stability analysis (Theorem 3).

IV. NUMERICAL EXPERIMENT

In this section, we present a series of numerical experiments to evaluate the accuracy, stability, and energy dissipation properties of the proposed KDF-SPH method when applied to the AC equation. All simulations employ the CN discretization for the linear term and explicit treatment of the nonlinear term, as described in scheme (38).

Example 1. We first consider the one-dimensional AC equation with Dirichlet boundary conditions on the domain [-10,10] over the time interval [0,T], with T=10:

$$\frac{\partial \mathbf{u}}{\partial t} = \Delta \mathbf{u} - \mathbf{f}(\mathbf{u}) \tag{53}$$

The exact solution is:

$$u(x,t) = \frac{1 + \tanh\left(\frac{3t}{4} - \frac{\sqrt{2}x}{4}\right)}{2}$$
 (54)

Figure 1 shows the energy evolution for different time steps. In Fig. 1(a) (dt = 2), the energy exhibits irregular oscillations, violating theoretical requirements. Fig. 1(b) (dt = 0.1) shows smooth monotonic decay, agreeing with Theorem 3's guarantee for $dt \le 1$. These results validate the $dt \le 1$ stability threshold.

Figure 2 demonstrates the MBP property under different time step sizes. In Fig. 2(a) with dt = 1 (violating the condition $dt \le 0.5$ in Theorem 2), the numerical solution exceeds the admissible range [-1,1], clearly breaking the MBP. Conversely, Fig. 2(b) with dt = 0.1 maintains strict bound preservation, with all solution values properly contained within [-1,1], in perfect accordance with Theorem 2. These contrasting results not only validate the sharp time-step constraint $dt \le 0.5$ for MBP preservation but also demonstrate that this theoretical bound is indeed optimal.

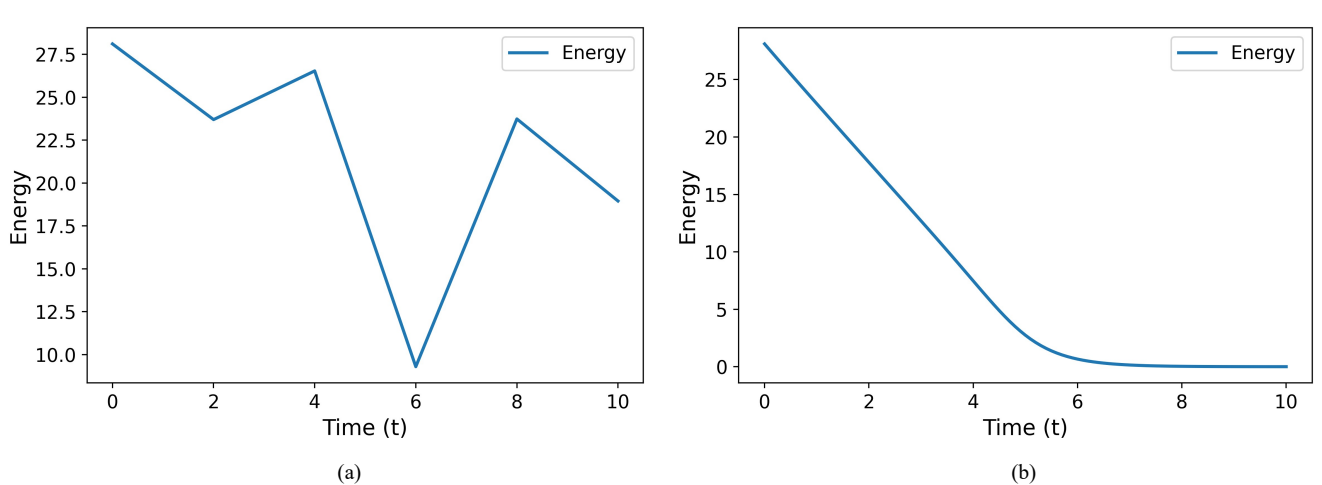


Fig. 1 Energy evolution at different time-steps in Example 1 (a) time-step dt = 2 and (b) time-step dt = 0.1

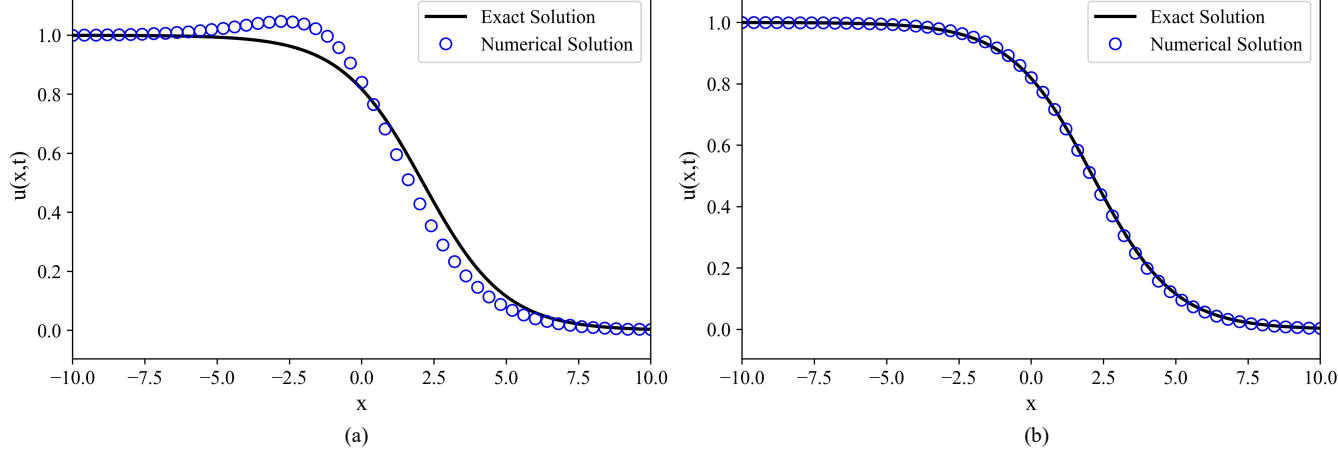
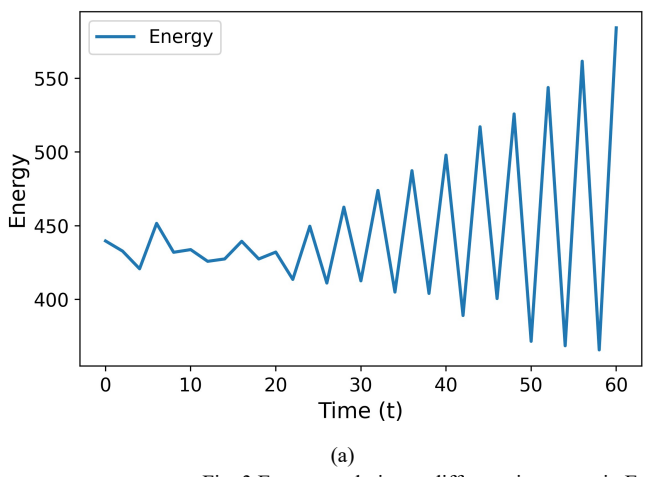


Fig. 2 Numerical solutions at different time-steps in Example 1 (a) time-step dt = 1 and (b) time-step dt = 0.1



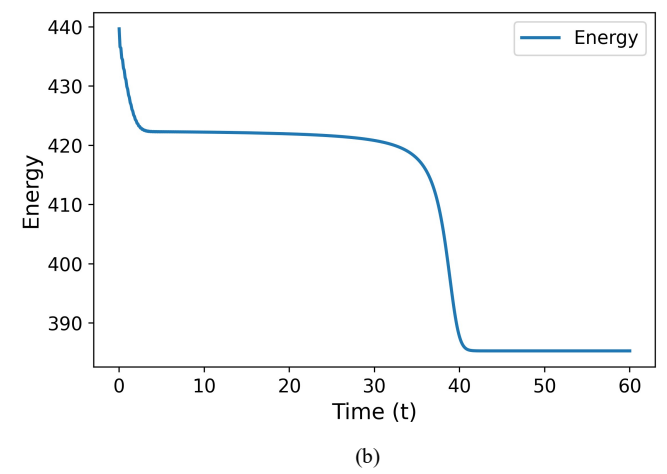


Fig. 3 Energy evolution at different time-steps in Example 2 (a) time-step dt = 2 and (b) time-step dt = 0.1

Example 2. Next, we test a more general one-dimensional problem with the initial condition and Dirichlet boundary conditions:

$$\frac{\partial \mathbf{u}}{\partial t} = \varepsilon^2 \cdot \Delta \mathbf{u} - \mathbf{f}(\mathbf{u})$$

$$\mathbf{u}(x,0) = 0.53x + 0.47\sin(-1.5\pi x)$$

$$\mathbf{u}(-1,t) = -1, \mathbf{u}(1,t) = 1$$
(55)

The parameter $\varepsilon = 0.1$, and the solution is computed over [0,T] with T=60. Figure 3 shows the discrete energy decreasing monotonically when $dt \le 1$, consistent with the energy law. For dt > 1, oscillations occur, indicating instability. These results confirm Theorem 3's dissipation condition. Figure 4 demonstrates smooth phase transitions converging to steady state

Table I compares the L_{∞} errors of numerical solution generated by both SPH and KDF-SPH in solving the one-dimensional AC equation at different spatial step sizes. The results demonstrate that KDF-SPH yields significantly smaller errors than SPH at the same spatial resolutions. Notably, KDF-SPH achieves a convergence order close to 2, which aligns with the theoretical analysis in III.D. These findings confirm the effectiveness of the proposed approach in solving the 2D AC equation, as it not only substantially reduces numerical errors but also improves convergence accuracy.

Example 3. We now consider the two-dimensional AC equation on $[0,2\pi]^2$ over the time interval [0,T] with T = 1:

$$\frac{\partial \mathbf{u}}{\partial t} = \Delta \mathbf{u} - \mathbf{f}(\mathbf{u}) + \mathbf{g}(x, t) \tag{56}$$

where g(x,t) is the source term, given by:

$$g(x,y,t) = (\pi^2 - 1) \cdot e^{-\pi^2 t} \cdot \sin(\pi x) \sin(\pi y)$$

$$+ \left[e^{-\pi^2 t} \cdot \sin(\pi x) \sin(\pi y) \right]^3$$
(57)

The exact solution is:

$$\mathbf{u}(x, y, t) = e^{-\pi^2 t} \cdot \sin(\pi x) \sin(\pi y) \tag{58}$$

Figure 5 confirms the method's spatial-temporal accuracy in capturing dynamics. Figure 7 shows excellent agreement between numerical and exact solutions, with smooth energy decay, validating the scheme's two-dimensional robustness and dissipation properties.

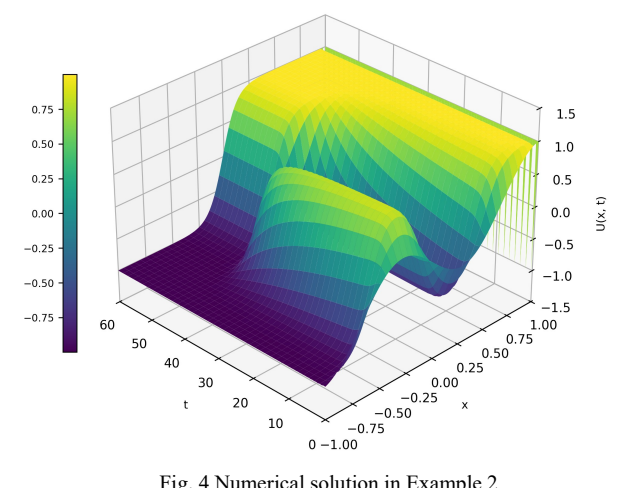


Fig. 4 Numerical solution in Example 2

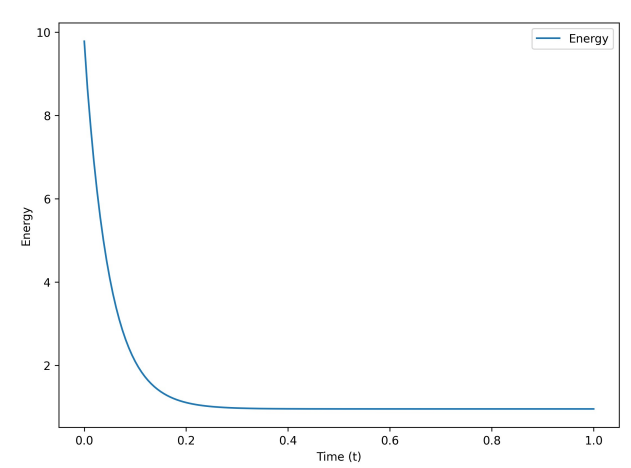


Fig. 5 The discretized energy functional in Example 3

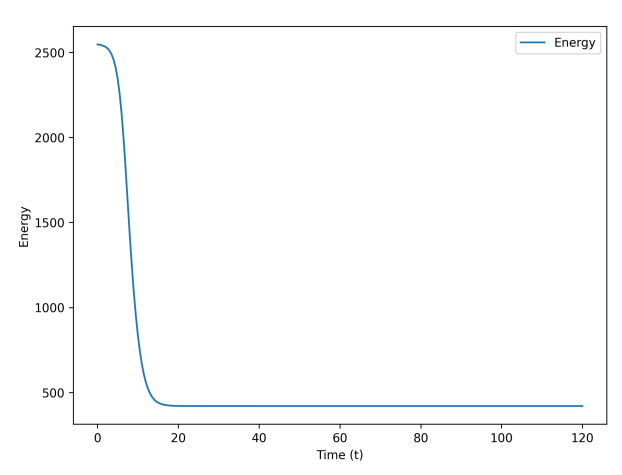


Fig. 6 The discretized energy functional in Example 4

Example 4. Finally, we examine the AC equation on $[0,2\pi]^2$ with initial condition and homogeneous Dirichlet boundary conditions:

$$\frac{\partial \mathbf{u}}{\partial t} = \varepsilon^2 \cdot \Delta \mathbf{u} - \mathbf{f}(\mathbf{u})$$

$$\mathbf{u}(x, y, 0) = 0.05 \sin x \cdot \sin y$$
(59)

The parameter $\varepsilon = 0.1$, and the solution is computed over [0,T] with T=120. This problem illustrates long-term behavior and asymptotic stability.

Figure 6 shows the energy dissipation evolution, decreasing monotonically with rapid initial changes ($0 \le t < 20$) before stabilizing (t > 20), confirming the method's long-time dissipation characteristics. Figure 8 presents numerical solutions at four time-instances: the interface evolves rapidly initially, showing clear phase transitions, then slows toward steady state. These results match theoretical predictions, validating the method's

accuracy for both transient and asymptotic behaviors.

The comprehensive numerical experiments presented above provide compelling and consistent evidence for the theoretical properties rigorously established in Sections III—IV.In particular, they clearly confirm the remarkable ability of the KDF-SPH scheme to preserve the MBP and maintain discrete energy dissipation under appropriate time-step constraints. The proposed method demonstrates superior robustness, excellent accuracy, and reliable stability across both one- and two-dimensional computational settings.

V. CONCLUSION

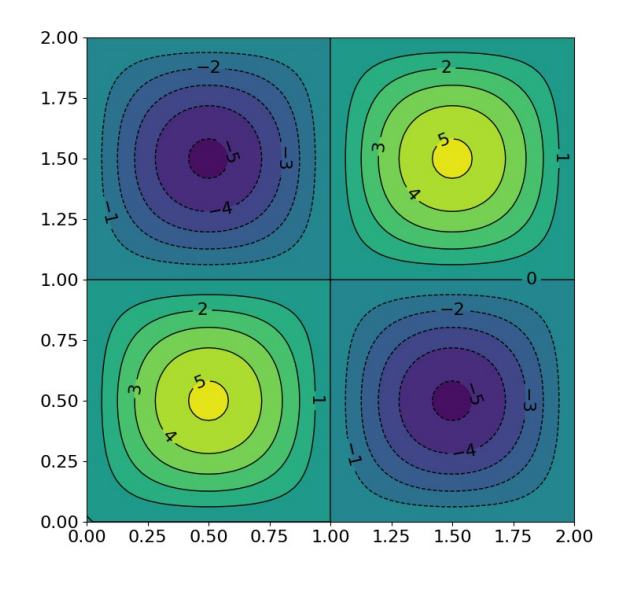
This paper proposes a novel framework for constructing numerical schemes that preserve both the MBP and energy dissipation for the AC equation. Within this framework, we develop a class of semi-implicit KDF-SPH schemes for the AC equation and rigorously analyze their stability properties.

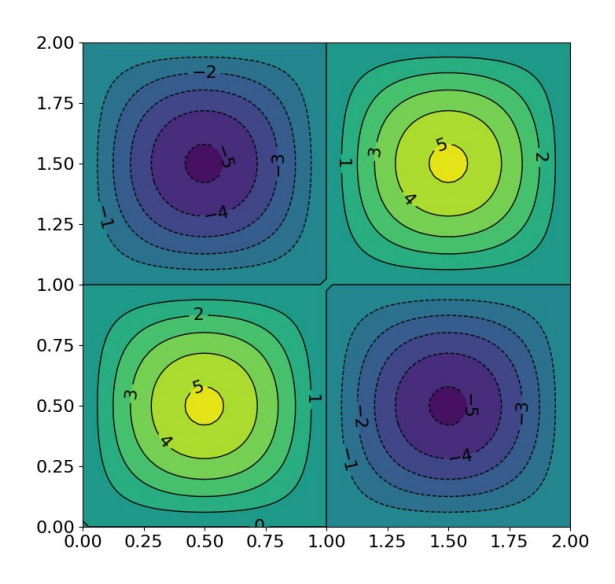
The main contributions are twofold:

- (i)Methodological Innovation: We pioneer the application of both standard and modified SPH methods to numerically solve the AC equation, with numerical experiments demonstrating their effectiveness.
- (ii)Theoretical Guarantees: We provide rigorous proofs that these schemes preserve discrete MBP and maintain energy stability, while achieving second-order convergence in space.

Although we focus on the classical AC equation, our framework extends the semi-linear parabolic equation theory proposed by Du et al. [18]. This generalization opens avenues for future work, including:

- (i) Applying the method to broader classes of equations.
- (ii)Developing unconditionally stable, higher-order accurate variants.





(b)

(a)
Fig. 7 Exact solution(a) and numerical solution(b) in Example 3

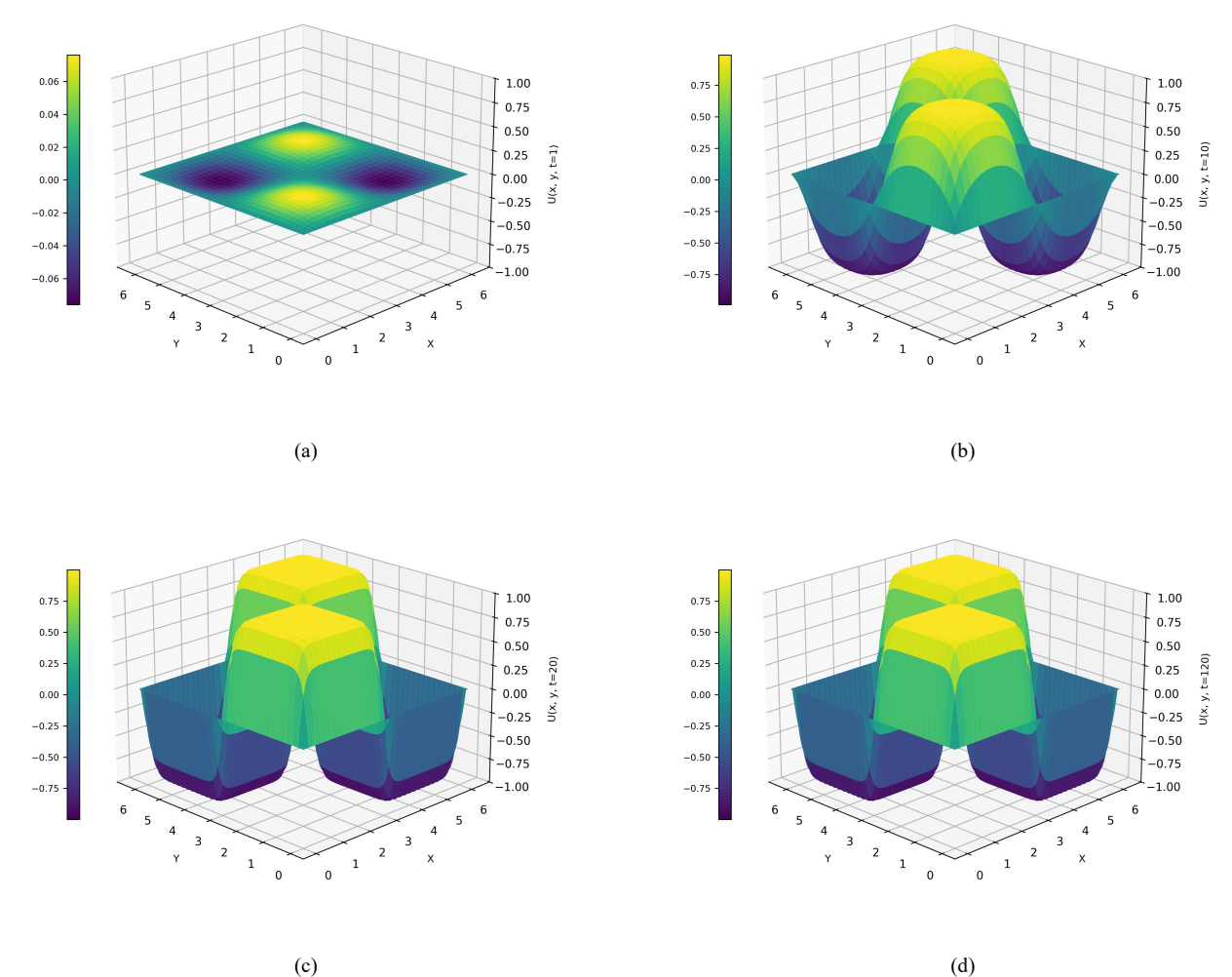


Fig. 8 Asymptotic behavior of the energy-stable scheme in Example 4 (a) t = 1 (b) t = 10 (c) t = 20 and (d) t = 120

 $\begin{tabular}{ll} TABLE I \\ Comparison of The L_{∞} Error for Example 2 \\ \end{tabular}$

Method	SPH		KDF-SPH	
	L_{∞}	$\log_2 \frac{\left(L_\infty ight)_{\Delta x}}{\left(L_\infty ight)_{\Delta x/2}}$	$L_{\scriptscriptstyle \infty}$	$\log_2 \frac{\left(L_{\infty}\right)_{\Delta x}}{\left(L_{\infty}\right)_{\Delta x/2}}$
$(\Delta x, \Delta y) = \left(\frac{1}{5}, \frac{1}{5}\right)$	0.00002891	-	0.00001538	-
$(\Delta x, \Delta y) = \left(\frac{1}{10}, \frac{1}{10}\right)$	0.00003520	-0.2840	0.00000415	1.8898
$(\Delta x, \Delta y) = \left(\frac{1}{20}, \frac{1}{20}\right)$	0.00003618	-0.0396	0.00000114	1.8640
$(\Delta x, \Delta y) = \left(\frac{1}{40}, \frac{1}{40}\right)$	0.00003651	-0.0130	0.00000035	1.7036

REFERENCES

- [1] Allen, Samuel M. and J. W. Cahn, "A microscopic theory for antiphase boundary motion and its application to antiphase domain coarsening," Acta Metallurgica, vol. 27, no. 6, pp. 1085-1095, 1979
- [2] Rasha I. H., Iqbal M. B., Mazin A., Iqbal H. Jebril, Ahmed B., Seddiki F. and Belal B., "On Stability Analysis of Nonlinear Systems," IAENG International Journal of Applied Mathematics, Vol. 55, no. 4, pp. 873-878,2025
- [3] X Chen, "Generation and propagation of interfaces for reaction-diffusion equations," Journal of Differential Equations, Vol. 96, no. 1, pp. 116-141, 1992
- [4] Fife, Paul C. and J. B. Mcleod, "A phase plane discussion of convergence to travelling fronts for nonlinear diffusion," Archive for Rational Mechanics & Analysis, vol. 75, no. 4, pp. 281-314, 1981
- [5] Lawrence, C., Evans Joel and Spruck, "Motion of level sets by mean curvature IV," Journal of Geometric Analysis, 1995
- [6] Shen J., "Modeling and numerical approximation of two-phase incompressible flows by a phase-field approach," 2011

- [7] Li, Y. and Kim J., "Energy stable schemes for Cahn-Hilliard equation with dynamic boundary conditions using SAV approach," Computer Methods in Applied Mechanics and Engineering, 2021
- [8] Budd J., Van Gennip Y. and Latz J., "Classification and image processing with a semi-discrete scheme for fidelity forced Allen-Cahn on graphs," 2020
- [9] Alsayed H., Fakih H., Miranville A. and Wehbe A., "Optimal control of an Allen-Cahn model for tumor growth through supply of cytotoxic drugs," Discrete and Continuous Dynamical Systems – S, vol. 15, no. 12, pp. 3481-3515, 2022
- [10] Wise S. M., Wang, C. and Lowengrub J. S., "An energy-stable and convergent finite-difference scheme for the phase field crystal equation," SIAM Journal on Numerical Analysis, 2009
- [11] Yang J., Yi N. and Zhang H., "High-order, unconditionally maximum-principle preserving finite element method for the Allen–Cahn equation," Applied Numerical Mathematics, vol. 62, no. 2, 2023
- [12] Wu J., Yang J. and Tan Z., "Unconditionally energy-stable time-marching methods for the multi-phase conservative Allen-Cahn fluid models based on a modified SAV approach," Computer Methods in Applied Mechanics and Engineering, 2022
- [13] Grave, Malu, and A. L. G. A. Coutinho, "Comparing the convected level-set and the Allen-Cahn phase-field methods in AMR/C simulations of two-phase flows," Computers & Fluids, 2022
- [14] Ghoneim Adam Yehudi, "A smoothed particle hydrodynamics-phase field method with radial basis functions and moving least squares for meshfree simulation of dendritic solidification," Applied mathematical modelling Pt.2, 2020
- [15] Guo Jia, Wang Haifeng and Hou Chenping, "An adaptive energy-based sequential method for training PINNs to solve gradient flow equations," 2024
- [16] Liu G. R., Liu M. B. and Li S., "Smoothed particle hydrodynamics a meshfree method," Computational Mechanics, vol. 33, no .6, pp. 491-491, 2004
- [17] Feng D. and Imin R., "A kernel derivative free SPH method," Results in Applied Mathematics, Vol. 17,2023
- [18] Du Q., Ju L., Li X. and Qiao Z., "Maximum Bound Principles for a Class of Semilinear Parabolic Equations and Exponential Time-Differencing Schemes," SIAM Review, 2021
- [19] Du Q., Ju L., Li X. and Qiao Z., "Maximum principle preserving exponential time differencing schemes for the nonlocal Allen-Cahn equation," Siam Journal on Numerical Analysis, vol. 57, no. 2, 2019
- [20] Shen J., Yang X., "Numerical approximations of Allen-Cahn and Cahn-Hilliard equations," Discrete & Continuous Dynamical Systems Series A, 2010